A THERMODYNAMIC AND KINETIC STUDY OF THE SOLIDIFICATION AND DECARBURIZATION OF MALLEABLE CAST IRON

TERMODINAMIČNA IN KINETIČNA ANALIZA STRJEVANJA IN RAZOGLJIČENJA BELEGA LITEGA ŽELEZA

Miran Pirnat[1], Primož Mrvar[2], Jože Medved[2]

[1]SIJ, Acroni, d. o. o, Jesenice, Slovenia,
[2]University of Ljubljana, Faculty of Natural Sciences and Engineering, Department of Materials and Metallurgy, Aškerčeva 6, 1000 Ljubljana, Slovenia
miran.pirnat@acroni.si

An analysis of the solidification and decarburization of white-heart malleable cast iron (MCI) is presented. The solidification and decarburization courses were examined with simple and differential scanning calorimetry. The microstructure characteristics and the physical properties of the white-heart malleable cast iron changed during the decarburization process. Also, the electrical resistivity changed with the change of carbon contents and the macro-and microstructures. Based on this hypothesis, a measuring method for simultaneous measurements of the electrical resistivity and dimensional variations during the decarburization process of white-heart malleable cast iron was developed. In addition, a physico-mathematical model was developed to follow the carbon concentration and to determine the depths of the decarburization zone during the decarburization process. The decarburization process was presented as a function of the specific electrical conductivity, the carbon concentration and the decarburization time.

Keywords: white-heart malleable cast iron (MCI), thermal analysis,electrical resistivity, specific electrical resistivity, decarburization time, depth of decarburization zone

Članek opisuje spremljanje strjevanja in razogljičenja belega litega železa. Potek strjevanja in razogljičenja sta bila preiskana z enostavno in diferenčno vrstično kalorimetrijo. Med procesom razogljičenja belega litega železa se spreminjajo značilnosti zgradbe in fizikalne lastnosti. Prav tako se zaradi spremembe koncentracije ogljika ter makro- in mikrostrukture spreminja tudi električna upornost. Na tej hipotezi je bila razvita merilna metoda istočasnega merjenja električne upornosti in dimenzijskih sprememb med procesom razogljičenja belega litega železa. Razvit je fizikalno-matematični model, s katerim je možno med procesom razogljičenja spremljati koncentracijo ogljika in določiti globino razogljičenja. Potek procesa razogljičenja je prikazan kot funkcija specifične električne upornosti, koncentracije ogljika in časa razogljičenja.

Ključne besede: belo lito železo, termična analiza, električna upornost, specifična električna upornost, čas razogljičenja, globina razogljičenja

1 INTRODUCTION

White-heart malleable cast iron (MCI) was prepared from a chilled hypoeutectic iron alloy. Afterwards, it was decarburized to achieve adequate mechanical properties. The morphology of the solidified phases, the temperature regions of the corresponding reactions and the formed phases were determined with a thermodynamic analysis of the MCI solidification and decarburization process. The fraction of pearlite and the heat treatment[1] are essential to obtain the desired properties of the MCI. The following methods were used to examine the solidification process and solid-state transformations: simple thermal analyses (TA), dilatometric analyses, and simultaneous thermal analyses (DSC). An "in situ" measuring apparatus, as a part of the laboratory equipment, was also developed to follow the electrical resistivity during the decarburization process. The goal of the examination was to design a model for the "in situ" monitoring of the decarburization process by determining the carbon concentrations and the depths of decarburization zone. The thermal analyses could be used for the quality control of the MCI, since it made it possible to determine the met-allurgical quality of the cast iron in the shortest possible time. The chemical composition and the nucleation conditions determined the obtained microstructure.[2–7] The simple thermal analysis made it possible to determine the reference liquidus temperature and the temperatures of the transformations and to forecast the latter properties of the castings.[8] In the solidification of the MCI it was important that all the remnant melt solidified entirely as a chill in the form of a cementite eutectic. The simple thermal analysis and dilatometric curves helped to examine the solidification process and the cooling of spheroidal-graphite cast iron (**Figure 1**).[9]

The as-cast MCI was decarburized in approximately 40 h in an oxidizing atmosphere at 1050 °C, when the cast microstructure changed with the reactions:

1. Formation of austenite:

$$(\alpha_{Fe} + Fe_3C) \rightarrow \gamma_{Fe}$$

2. Decomposition of cementite:

$$Fe_3C \rightarrow 3\gamma_{Fe} + C_{(malleablizedgraphite)}$$
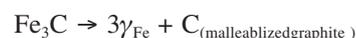
3. Decarburization process:
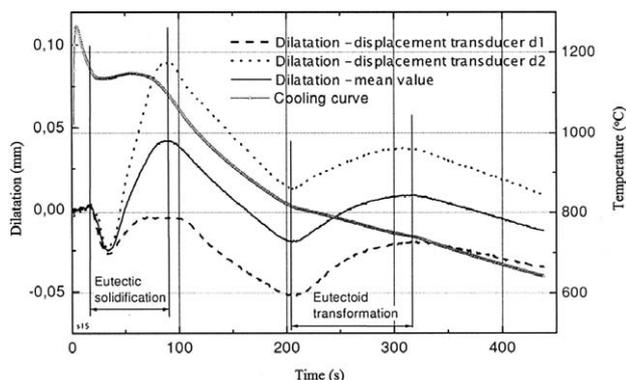
Figure 1: Cooling curve and dilatometric curves of slightly hypo-eutectic spheroidal graphite cast iron[9]
Slika 1: Ohlajevalna krivulja in dilatometrske krivulje podevtektske sive litine s kroglastim grafitom[9]

$C_{(malleablized\ graphite)}$ and $[C]_\gamma + H_2O_{(g)} = CO_{(g)} + H_{2(g)}$
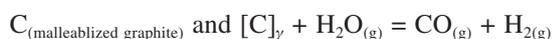
4. Precipitation of ferrite:

$$\gamma_{Fe} \rightarrow \alpha_{Fe}$$

5. Formation of pearlite:

$$\gamma_{Fe} \rightarrow (\alpha_{Fe} + Fe_3C)$$
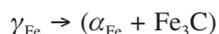
6. Precipitation of graphite:

$$\alpha_{Fe} \rightarrow Graphite_{(tertiary)}$$
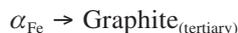
The decarburization proceeded predominantly by the reactions:

$$[C]_{\gamma-Fe} + H_2O_{(g)} = CO_{(g)} + H_{2(g)} \quad (1)$$

and

$$C_{malleablized\ graphite} + H_2O_{(g)} = CO_{(g)} + H_{2(g)} \quad (2)$$
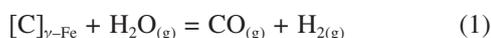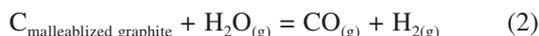
The decarburization process of steel, such as electrical steel,[10,11] proceeded by the decarburization reaction (1). The decarburization process of MCI started with a carbon loss in austenite, $[C]_{\gamma-Fe}$ (reaction 1), and then it was continued by $C_{malleablized\ graphite}$ loss according to reaction (2) after the cementite decomposed according to reaction:

$$Fe_3C = 3\gamma_{Fe} + C_{malleablized\ graphite} \quad (3)$$

The decarburization process depends on the chemical composition of the decarburized material (steel or MCI), on the applied atmosphere,[10,11] the temperature and first of all on the wall thickness of the casting. For MCI it was also essential to know how the microstructure was influenced by the wall thickness.[12] The relationship between the mass fraction of carbon and the decarburization time is presented in **Figure 2**. The decarburization was achieved by annealing in the temperature range from 1070 °C to 1075 °C in a gas atmosphere with water vapor ($H_2O_{(g)}$), and the process consisted of carbon diffusion from the interior towards the surface of the MCI casting, of the water vapor transport to the surface of the MCI casting, the oxidation of MCI carbon on the surface of the MCI casting where proceeded and also the oxidation
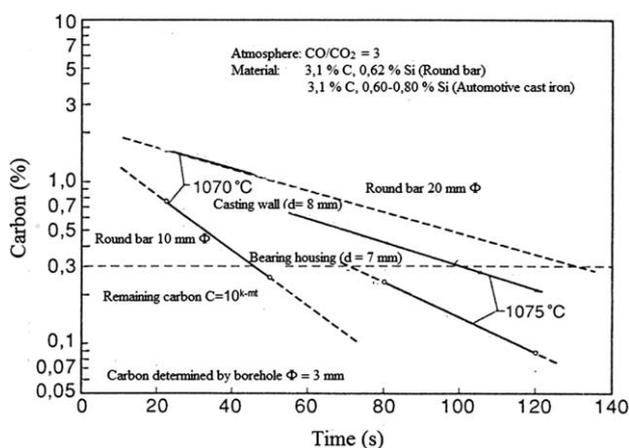
Figure 2: Relationship between the mass fraction of carbon and the decarburization time[12]
Slika 2: Odvisnost masnega deleža ogljika od časa razogljičenja[12]

of iron and of the other elements. The relations between the decarburization time and the remaining carbon concentration in the MCI are represented by the following equations:[12]

$$\lg C = k - m \cdot t \quad (4)$$

$$C = 10^{k - m \cdot t} \quad (5)$$

$$t = \frac{k - \lg C}{m} \quad (6)$$

with:
C – remaining carbon concentration,
t – time,
k, m – constants

The microstructural characteristics and the physical properties of the malleable cast iron changed during the decarburization process. Due to changed carbon concentrations and changed macro- and microstructures the electrical resistivity also varied. The relationship between the electrical resistivity and the specific electrical resistivity applied for the calculations of the specific electrical resistivity during the MCI decarburization process are described with the equation:

$$\rho = R \frac{A}{l} \ (\Omega\ m) \quad (7)$$

where:
ρ = specific electrical resistivity of the specimen (Ω m)
R = electrical resistivity of the specimen (Ω)
A = cross-section of the specimen (mm²)
l = length (mm)

Matthiessen's rule[13] describes the relation between the specific electrical resistivity and the temperature, as follows:

$$\rho(T) = \rho_0 + \rho_G(T) \quad (8)$$

where ρ_0 is a term that is independent of the temperature and takes into account the influence of the alloying elements and $\rho_G(T)$ is a temperature-dependent term.

2 EXPERIMENTAL

"In-situ" simple thermal and dilatometric analyses of the same alloy were made in industrial conditions. The "in-situ" measuring equipment is presented in **Figure 3**.[14]

A sample for chemical analysis was taken after each measurement and for laboratory decarburization. For an easier comparison, some of those specimens were decarburized together with industrial castings in industrial conditions, while the others were prepared only for laboratory decarburization tests. The chemical analyses of the as-cast cast irons and of the decarburized specimens were made after "in-situ"dilatometrical measurements, thermal analyses and differential scanning calorimetry to follow how the electrical resistivity varied during the laboratory decarburization process.The chemical compositions of the as-cast cast iron samples were evaluated and are presented in **Tables 1 and 2**.

The measurements of the electrical resistivity and of the dimensional changes were performed with laboratory equipment to follow the variations of the electrical resistivity of the MCI specimens during the decarburization process at 1050 °C, 1075 °C and 1100 °C for periods of (12, 24 and 48) h in atmospheres of argon, CO_2, N_2 and N_2 + H_2O. **Figure 4** shows the used equipment.

The Olympus BX 1 optical microscope with the DP 70 video camera and the analySIS 5.0 software for analyzing micrographs was used in the metallographic ex-

Figure 4: Laboratory equipment for measuring electrical resistivity, and performing dilatometric analyses during the decarburization process
Slika 4: Posnetek naprave za izvedbo meritev električne upornosti in dilatometrijske analize pri razogljičenju

aminations. Multiple image alignment (MIA), a method of stitched overview, was applied to determine the microstructural constituents and the variation of their fractions with the distance from the surface of the specimens. The microstructural components were determined across the specimen's cross-section from the center ($x = 0$) towards the edge ($x = 2\ 500$ μm). The distance from the center to the edge of the specimens decarburized in laboratory conditions was divided into five sections, each was 500 μm long. The microstructural changes and the variations in the microstructural constituents were determined in each section. Afterwards, the single pictures were stitched into a joint picture.

3 RESULTS AND DISCUSSION

The simple thermal analysis was applied to record the cooling curves and the curves of the dimensional changes of specimens Nos. 1, 2, 3 and 4. In addition, characteristic temperatures of the solidification and of the transformations were determined, too. The cooling curve with the marked characteristic temperatures for the

Figure 3: Equipment for "in situ" simple thermal and dilatometric analyses with the measuring cell[14]
Slika 3: Naprava za enostavno termično in dilatometrijsko analizo z merilno celico[14] "in situ"

Table 1: Chemical compositions of as-cast cast iron samples, including the C+Si sum and the Mn/S ratio w/%
Tabela 1: Kemijska sestava vzorcev 1, 2, 3, 4, vsota C + Si in Mn/S v masnih deležih

Chemical composition in mass fractions, w/%								
Sample	C	Si	Mn	S	Al	P	Cr	C+Si	Mn/S
1.	2.8405	0.9174	0.5026	0.1952	0.0010	0.0321	0.0395	3.7579	2.5748
2.	3.0633	0.9549	0.5005	0.1879	0.0024	0.0321	0.0396	4.0182	2.6637
3.	3.0032	0.9305	0.4991	0.2132	0.0009	0.0323	0.0398	3.9337	2.3410
4.	3.0259	0.9368	0.5045	0.1818	0.0004	0.0312	0.0040	3.9627	2.7750

Table 2: Chemical compositions of as-cast cast iron samples prepared for laboratory decarburization, including the C+Si sum and the Mn/S ratio
Tabela 2: Kemijska sestava vzorcev belega litega železa za razogljičenje z vsoto C + Si in razmerjem Mn/S v masnih deležih, w%

Chemical composition in mass fractions, w/%								
C	Si	Mn	S	Al	P	Cr	C+Si	Mn/S
2.99	0.85	0.49	0.17	0.004	0.0321	0.04	3.84	2.88

specimen No. 3 is presented in **Figure 5**. It shows that the solidification started at 1280 °C with the precipitation of primary austenite (L → γ_{Fe}) and continued until the temperature of the eutectic reaction (L → (γ_{Fe} + Fe₃C)) at 1154 °C. After the eutectic reaction was completed, the cooling continued in the solid state down to the eutectoid reaction (γ_{Fe} → (α_{Fe} + Fe₃C)) at 740 °C. Afterwards, the cooling continued and no further changes were detected on the cooling curve. The liquidus and solidus temperatures of all the specimens, i.e., of Nos. 1, 2, 3 and 4, were collected and are presented in **Table 3** with the results of the differential scanning calorimetry. Next to characteristic temperatures, the reaction enthalpies were determined also.

Figure 6a presents the heating curves of industrially cast specimens, i.e., of the initial specimen, and of the decarburized specimen with 0.18 % C. Both curves exhibit the exothermic and endothermic peaks of the eutectoid transformation (γ_{Fe} → α_{Fe} + Fe₃C); (α_{Fe} + Fe₃C → γ_{Fe}) at 757 °C and 752 °C. Both peaks were much more pronounced with the initial specimen since the enthalpy of transformation was –16.48 J/g, while the enthalpy of transformation in the decarburized specimen was much smaller, only –3.632 J/g. The melting of the initial specimen (blue line) commenced at 1139 °C with the solidification of the (γ_{Fe} + Fe₃C → L) eutectic, and it continued with the melting of the primary austenite (γ_{Fe} → L) at 1188 °C.

The melting enthalpy was at –1 34.2 J/g. In the decarburized specimen (red line) no melting of the eutectic (γ_{Fe} + Fe₃C → L) was detected. After the eutectoid transformation (α_{Fe} + Fe₃C → γ_{Fe}) at 752 °C, the heating was continued until the primary austenite melted (γ_{Fe} → L) at 1 331 °C, then the peritectic reaction (γ_{Fe} + L → δ_{Fe}) proceeded at 1 452 °C and the δ-ferrite melted (δ_{Fe} → L) at 1 479 °C.
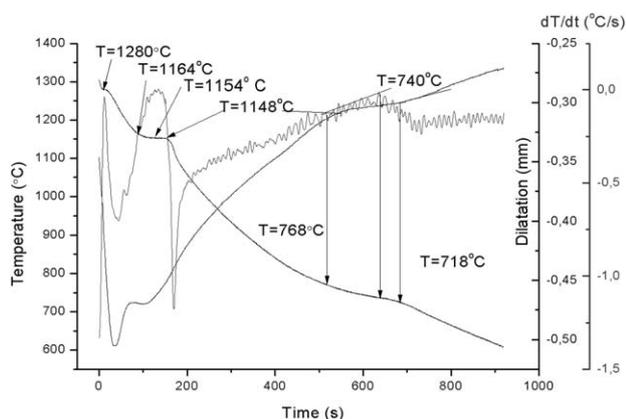
Figure 5: Dilatometric and cooling curve and derivative of the cooling curve with marked temperatures of the solidification start, of the eutectic solidification and of the eutectoid transformation for sample No. 3
Slika 5: Dilatometrijska in ohlajevalna krivulja z odvodom ohlajevalne krivulje s temperaturami začetka in evtektičnega strjevanja ter evtektoidne premene za vzorec 3
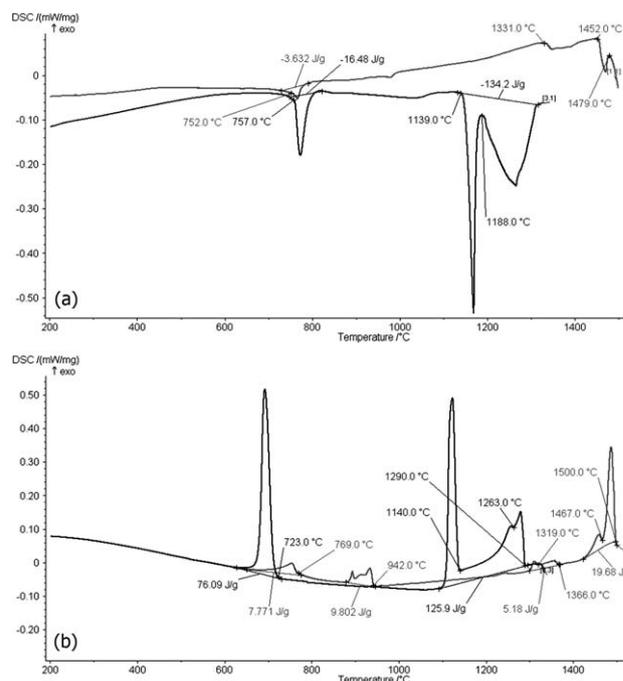
Figure 6: Heating (a) and cooling curves (b) of the as-cast specimen (blue), and specimen with mass fraction of C 0.18 %, decarburized in industrial conditions (red), obtained by differential scanning calorimetry
Slika 6: a) Segrevalni in b) ohlajevalni krivulji diferenčne vrstične kalorimetrije; modro: izhodno lito stanje; rdeče: industrijsko razogljičeni vzorec z masnim deležem C 0,18 %

Figure 6b presents the cooling of the initial (blue line) and of the decarburized specimen (red line). The solidification of the decarburized specimen started at 1500 °C with precipitation of the δ-ferrite (L → δ_{Fe}). The peritectic reaction (δ_{Fe} + L→ γ_{Fe}) at 1467 °C, at 1366 °C the peak of formation of primary austenite (L → γ_{Fe}), at 942 °C the peak of formation of hypoeutectoid ferrite from austenite (γ_{Fe} → α_{Fe}) and at 769 °C a smaller peak of eutectoid transformation (γ_{Fe} → α_{Fe} + Fe₃C) were detected. The melting enthalpy was 19.68 J/g, and of eutectoid transformation 7.771 J/g.

The solidification of the basic specimen started at 1290 °C with the precipitation of the primary austenite (L → γ_{Fe}) and it was completed at 1140 °C with eutectic reaction or the solidification of the eutectic (L → γ_{Fe} + Fe₃C), respectively. At 723 °C a big exothermic peak of eutectoid transformation (γ_{Fe} → α_{Fe} + Fe₃C) appeared. The enthalpy of solidification was 125.9 J/g, and of eutectoid transformation was 76.09 J/g.

Figure 7 shows the results of measurements of the electrical resistivity and of the dimensional changes during decarburization of specimen No. 8. The decarburization proceeded at 1100 °C for 12 hours in the N₂+H₂O atmosphere. The obtained value of the electrical resistivity after heating to the decarburization temperature of 1100 °C was 0.2725 Ω and it was constantly dropping as the decarburization continued. After 40 000 s of decarburization, the electrical resistivity dropped to 0.2525 Ω.

Table 3: Characteristic temperatures obtained with simple thermal analysis (TA) and differential scanning calorimetry (DSC) in °C
Tabela 3: Značilne temperature TA in DSC v stopinjah Celzija

Solidification and phase transformations in solid state	Temperatures of solidification and phase transformations in solid state					
	TA				DSC	
	Specimen				Decarburized specimen in industrial conditions, containing mass fraction of C 0.18 %	As-cast specimen
	1	2	3	4		
L → δ_{Fe}					1 500	
δ_{Fe} + L → γ					1 467	
L → γ_{Fe}		1 280	1 280	1 281	1 366	1 290
L → (γ_{Fe} + Fe$_3$C)	1 158	1 154	1 154	1 154		1 140
γ_{Fe} → α_{Fe}					942	
γ_{Fe} → α_{Fe} + Fe$_3$C)	740	738	740	733	769	723

With a lowering of the electrical resistivity dimensional changes occurred. The dimensional changes dropped from 400 μm at the beginning of the decarburization process to 120 μm at the end of the process.

Figure 8 presents the changes of the microstructure and of the fractions of the microstructural constituents as a function of the distance x from the center of the specimen to its edge. The stitched metallographic image presents the microstructures and the fractions of the microstructural constituents, i.e., pearlite, ferrite, and graphite. The fractions of microstructural constituents are also presented graphically as a function of the distance x from the specimen center to its edge. The fraction of microstructural constituents changed from the center to the edge and greater changes of the microstructural constituents were detected at adistance of 1 000 μm to 1 500 μm from the center. The fraction of graphite was reduced to 1 % and the fraction of pearlite to 70 %. In contrast, the fraction of ferrite was constantly increasing and the share of ferrite was 25 % at adistance of 1 500 μm, while its share at the edge of the specimen reached as high as 90 %.

Based on measurements of the electrical resistivity and the changed lengths of specimens during the decarburization of white-heart cast iron and applying a physico-mathematical model of white-heart cast iron decarburization, variations of the carbon concentrations and the specific electrical resistivity during the decarburization process were evaluated as a function of the decarburization time. The variations of the carbon concentrations were calculated for (12, 24, 36, 48 and 60) h of decarburization at a temperature T = 1 000 °C for specimens that were decarburized in various atmospheres. These relations are presented in **Figure 9**. The relations between the decarburization time and the depths of the decarburized zone are shown in **Figure 10**. It is evident from the plot in **Figure 9** that the greatest variations of the specific electrical resistivity and of the carbon concentration occurred between 12 h and 24 h of decarburization. A similar behavior was also found with measurements of the electrical resistivity of laboratory specimens, where the corresponding time interval was between 11.1 h and 22.2 h. The course of the decarburization process in **Figure 9**, i.e., the relation between the carbon concentrations and the time of decarburi-
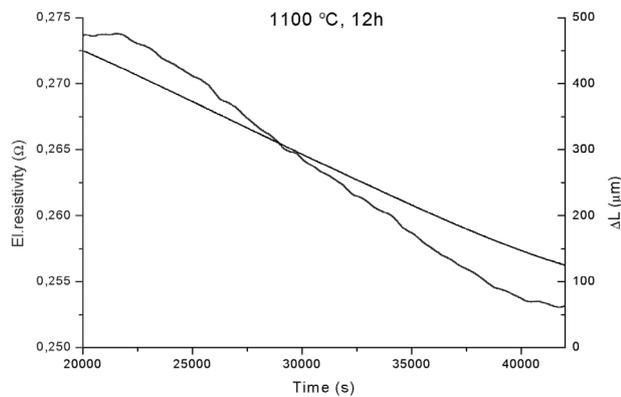
Figure 7: Variations of electrical resistivity and dimensional changes with time during decarburization of the specimen, decarburized in laboratory conditions (T_3 t_1); T = 1 100 °C, 12 h, N$_2$ + H$_2$O mixture,
Slika 7: Električna upornost in dimenzijske spremembe v odvisnosti od časa razogljičenja za vzorec (T_3 t_1); T = 1 100 °C;12 h; N$_2$ + H$_2$O
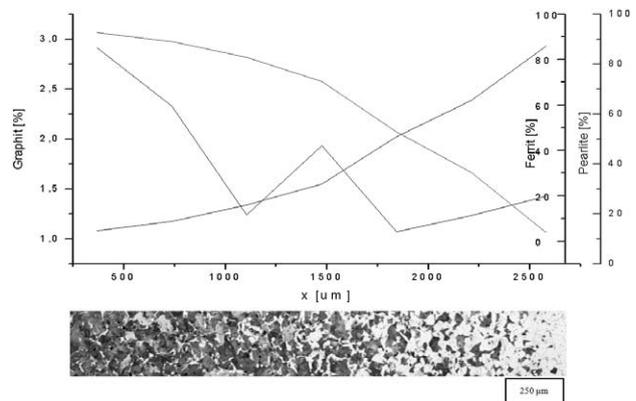
Figure 8: Micrograph with microstructural constituents in the specimen (T_3 t_1);T = 1 100 °C; 12 h; N$_2$ + H$_2$O mixture
Slika 8: Posnetek mikrostrukture in deleži mikrostrukturnih sestavin vzorca (T_3 t_1) ; T = 1 100 °C; 12 h; N$_2$ + H$_2$O
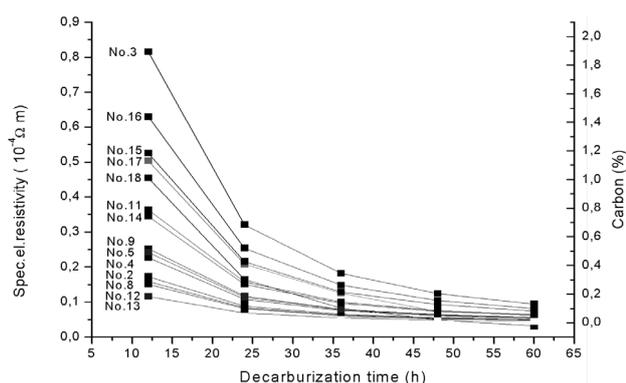
Figure 9: Variation of the carbon concentration and of the specific electrical resistivity during the decarburization process at $T = 1\ 100$ °C
Slika 9: Sprememba koncentracije ogljika in specifične električne upornosti v odvisnosti od časa razogljičenja pri temperaturi $T = 1\ 100$ °C

Figure 10: Variation of the depth of the decarburization zone during the decarburization process at $T = 1\ 100$ °C
Slika 10: Sprememba globine razogljičenja v odvisnosti od časa razogljičenja pri temperaturi $T = 1\ 100$ °C

zation, was similar to that described where the decarburization of the electrical sheet was investigated[15]. Furthermore, **Figure 10** shows that an increased decarburization rate in the time interval between 12 h and 24 h of decarburization resulted in greater depths of the decarburized zone that varied between 1 mm and 6 mm, depending on the decarburization time and the decarburization conditions. The relationships between the wall thickness of the casting and the decarburization time at T = 1 000 °C are presented, showing that a depth of the decarburization zone of 5 mm was reached after 50 h of decarburization.[12]

The temperature of the solidification and of the phase transformations were determined by analyzing the course of the MCI solidification and decarburization by physico-metallurgical means. Among those temperatures, the essential in the MCI decarburization process is the temperature of eutectoid transformation ($\gamma_{Fe} \rightarrow \alpha_{Fe} + Fe_3C$) at 752 °C.

The mechanism of the MCI decarburization process was determined. This process started at $T \geq 752$ °C by carbon loss in the austenite, $[C]_{\gamma\text{-Fe}}$, and was continued by $C_{malleablized\ graphite}$ loss, described with the reactions:

$$[C]_{\gamma\text{-Fe}} + H_2O_{(g)} = CO_{(g)} + H_{2(g)}, \text{ and}$$

$$C_{malleablized\ graphite} + H_2O_{(g)} = CO_{(g)} + H_{2(g)}$$
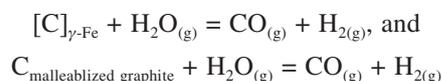
4 CONCLUSIONS

In the first part of the research, the MCI decarburization was investigated with the thermal analyses, chemical analyses, and differential scanning calorimetric analyses of as-cast malleable samples. The thermal analyses revealed the entire course of the solidification process, the course of the cooling, and reactions relating to how the austenite, cementite eutectic and pearlite were formed. Differential scanning calorimetry of the as-cast specimens confirmed the course of the reactions that were determined by the thermal analysis.
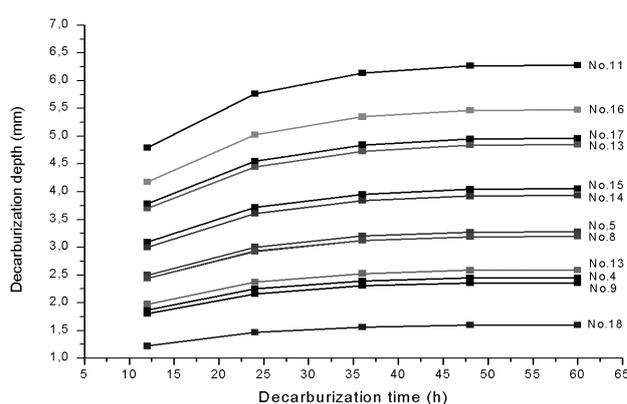
Further examinations were focused on a laboratory examination of the malleablizing process from the thermodynamic and kinetic points of view and the dilatometric analyses of specimens during the malleablizing process were performed. The measurements of the electrical resistivity were added to follow the decarburization process more precisely. Electrical resistivity changes during the decarburization process of the specimens decarburized in laboratory conditions were confirmed by an assessment of the changes in the microstructures.

5 REFERENCES

[1] P. V. Hübner, G. Pusch, O. Liesenberg, O.; R. Döpp, R., Bruch-mechanische Kennwerte von entkohlendgeglühtemTemperguss, Giesserei, 90 (**2003**) 5, 82–92

[2] M. J. Oliveira, L. F. Malheiros, C. A. Silva Ribeiro, Evaluation of the heat of solidification of cast irons from continuous cooling curves, Journal of Materials Processing Technology, 92–93 (**1999**), 25–30

[3] P. Mrvar, M.Trbižan, J. Medved, Solidification of Aluminium Cast Alloys investigated by the Dilatation Analysis, Metalurgija, 40 (**1985**), 81–84

[4] P. Mrvar, J. Medved, A. Križman, Control of Microstructure during the Eutectoid Transformation in the As-cast Spheroidal Graphite Cast Iron with "in-situ" Dilatation Analysis and Quenching Experiments, Steel Research Int., 77 (**2006**) 5, 353–361

[5] J. Medved, P. Mrvar, Thermal Analysis of the Mg-Al Alloys, Materials Science Forum, 508 (**2006**), 603–608

[6] P. Mrvar, M. Trbižan, J. Medved, A. Križman, Study of the Eutectoid Transformation in the As-cast Spheroidal Graphite Cast Iron with »in-situ« Dilatation Analysis-Method for Quality control, Materials Science Forum, 508, (**2006**), 287–294

[7] E. Guhl, O. Liesenberg, R. Döpp, Qualitätskontrolleniedriglegierter-Gußeisenschmelzen durchrechnergestütztethermische Analyse, Giessereiforschung, 46 (**1994**) 2/3, 62–70

[8] W. Menk, M. O. Speidel, R. Döpp, Die thermische Analyse in der Praxis der Eisen- und Tempergießerei, Giessereiforschung 44 (**1992**) 2, 66–79

[9] P. Mrvar, M. Trbižan, J. Medved, Dilatation analysis of the eutectoid transformation of the as-cast spheroidal graphite cast iron, Scandinavian Journal of Metallurgy, 31 (**2002**), 393–400

[10] D. Steiner Petrovič, Non-oriented electrical steel sheets, Mater. Tehnol., 44 (**2010**), 317–325

[11] D. Steiner Petrovič, B. Markoli, M. Čeh, The nanostructure of non-oriented electrical steel sheets, Journal of Magnetism and Magnetic Materials, doi 10.1016/j.jmmm.2010.05.026

[12] J. Beer, H. Hocke, Das Glühen von schweißbarem Temperguß – EinBerichtaus der Praxis, Giesserei 82 (**1995**) 3, 87–90

[13] E. Hornbogen, H. Warlimont, Metallkunde, Aufbau und Eigenschaften von Metallen und Legirungen, 2. Auflage, Springer Verlag, Berlin, Heidelberg, New York, (1996)

[14] P. Mrvar, M. Trbižan, J. Medved, Investigation of cast iron solidification with dilatation analysis, Kovine Zlit. Tehnol. 33, (**1999**) 1–2, 45–49

[15] K. M. Marra, E. A. Alvarenga, V. T. L. Buono, Decarburization kinetics during annealing of a semi-processed electrical steel, ISIJ International, 44 (**2004**) 3, 618–622